

High-speed two-frame shadowgraphy for velocity measurements of laser-induced plasma and shock-wave evolution

Peter Gregorčič* and Janez Možina

Faculty of Mechanical Engineering, University of Ljubljana, Aškerčeva 6, 1000 Ljubljana, Slovenia

*Corresponding author: peter.gregorcic@fs.uni-lj.si

Received March 1, 2011; revised May 9, 2011; accepted June 18, 2011;

posted June 22, 2011 (Doc. ID 143509); published July 20, 2011

We describe a high-speed, two-frame shadowgraph method for the two-dimensional visualization of an expanding laser-induced plasma and shock wave in two time instances. The developed experimental method uses a 30 ps, green-laser, polarized pulse for the direct and delayed illumination separated by a variable time delay in the range from 300 ps to 30 ns. Since the exposed images of a single event are captured with two CCD cameras, the established method enables velocity measurements of the fast laser-induced phenomena within the nanosecond excitation-laser pulse as well as at later times—when the excitation-laser radiation has already ended. © 2011 Optical Society of America

OCIS codes: 120.4820, 140.3440, 320.4240.

During laser–material interaction, a plasma plume is generated when there are sufficiently high laser-pulse intensities [1]. This results in a microexplosion, which produces a shock wave that propagates into the surrounding medium. Since the propagating shock wave contains important information about the laser–material interaction [2], a detailed, spatially and temporally resolved characterization of the laser-induced plasma and the shock wave is of great importance in various medical [3,4] and industrial applications [5–7].

The methods used in the characterization of laser-induced plasma and shock waves include different optical techniques, such as shadow and streak photography [8–11], holography [12], laser-beam-deflection probe [13], interferometry [14], and laser-induced spectroscopy [15,16]. Since the plasma and ablative shocks are short, transient phenomena that exhibit significant pulse-to-pulse variations, there is a special interest in methods that provide their spatially and temporally resolved characterization [17]. A laser-beam-deflection probe, for example, can provide temporally resolved detection at a single point in space, while shadow photography is capable of capturing two-dimensional (2D) spatially resolved information at a single moment [13]. On the other hand, ultrahigh-speed 2D shadowgraphy [18] and holographic recording [12,19] make possible measurements of spatially resolved information in a limited number of time instances, but require a very complex environment.

A great interest in instantaneous-velocity measurements of plasma and shock waves produced by high-intensity, nanosecond laser pulses arises from many laser-assisted applications, where the shock-wave peak pressure, which is related to the shock-wave propagation speed [10,20], is a crucial parameter. Since these expansion velocities exceed 100 km/s [21,22], successive 2D images of a single event should be captured in a time interval shorter than 1 ns. In addition, to get insight into the development of plasma within the few-nanosecond-excitation-laser pulse, time delays below 1 ns are also mandatory.

In this Letter we present a new high-speed, two-frame shadowgraphy that enables 2D visualization of a single optical breakdown event in two time instances. The developed method has a variable delay between the direct and the delayed 30 ps illumination, in the range between 300 ps and 30 ns. The capability of the presented method is demonstrated by velocity measurements of the laser-induced plasma and the shockwave in air.

The experimental setup is schematically shown in Fig. 1. A Q-switched Nd:YAG laser ($\lambda = 1064$ nm, Quantel, France, Brio) is employed as the excitation laser. It emits 4 ns (FWHM) pulses with energy of 14 mJ after the attenuator (A). The pulse is detected by the fast 1 GHz photodiode (PD1). The excitation beam is guided through the beam expander (BE) and focused to a diameter of 50 μm in air under standard conditions. As the illumination source, we used a frequency-doubled Nd:YAG laser ($\lambda = 532$ nm, Ekspla, Lithuania, PL2250-SH-TH) with a pulse duration of 30 ps. After the half-wave plate (HWP), the beam polarization forms a 45° angle with respect to the optical table. The polarizing beam splitter (PBS) transmits the x -polarization (the direct beam) and reflects the y -polarization (the delayed beam) into the delay line. The path of the delayed pulse is 0.1–10 m longer than the path of the direct pulse. In this way, we can produce an arbitrary time delay, Δt , in the range between

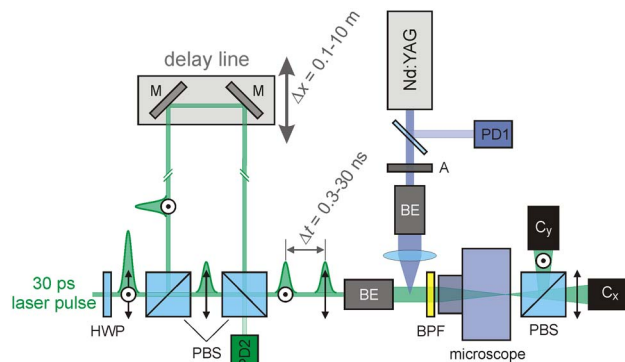


Fig. 1. (Color online) Experimental setup of the high-speed, two-frame shadowgraphy.

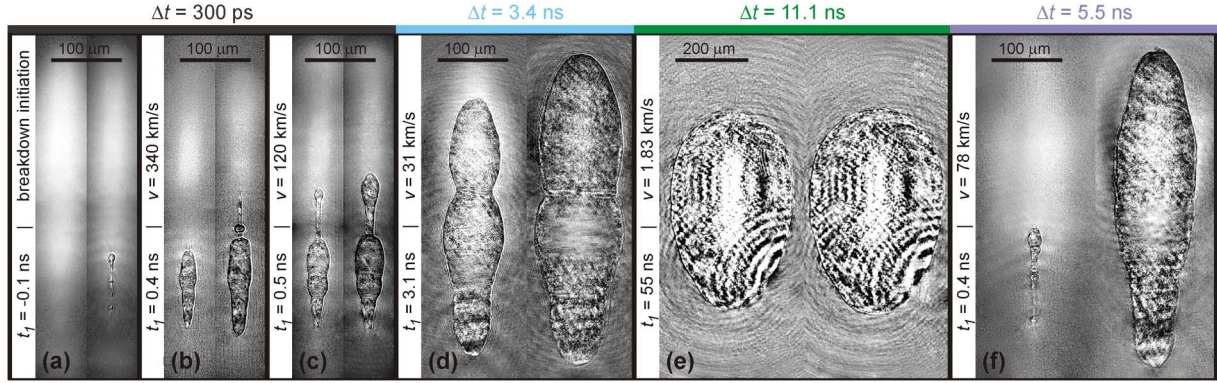


Fig. 2. (Color online) Typical pairs of images captured during the independent breakdown events (at different times, t_1) and with different delays, Δt . The excitation-laser beam is entering from the top. The scale is shown with the black bar.

300 ps and 30 ns. Here, the shortest time delay, Δt , is theoretically limited by the illumination-pulse duration, but practically it should be at least 1 order of magnitude longer. If a shorter delay line is required due to higher velocities of the observed phenomena, a shorter illumination pulse should be used.

The illumination pulses are detected with the photodiode (PD2) placed behind the second PBS, which combines the direct and delayed pulses into the same path. Before the illumination of the laser-induced phenomena, both pulses are expanded with the BE. A narrow band-pass filter (BPF) centered at 532 nm is placed between the breakdown region and the microscope to block the light emitting from the plasma. Another PBS is placed inside the microscope, where it divides the direct (x -polarized) pulse to the camera C_x and the delayed (y -polarized) pulse to the camera C_y , so two 2D images of a single event at two time instances are captured with inexpensive CCD cameras (Basler AG, Germany, scA1400-17fm, 1.4 Mpx). The lasers and the cameras are synchronized with a pulse generator connected to a personal computer, allowing an electronic variation in the delay between the excitation and the illumination laser pulses. The experimental setup is automatically controlled with specially developed software that also enables data acquisition from a digital oscilloscope as well as image acquisition and the subpixel alignment of captured images and subsequent image processing.

The presented method can be used for instantaneous-velocity measurements and for a threshold analysis of the laser-induced breakdown. To demonstrate this, we measured the evolution of the laser-induced plasma and the shock wave in air with different delays, Δt , between the direct and the delayed illumination. Typical pairs of images captured during an independent breakdown event and using different delays, Δt , are shown in Fig. 2. The measured velocities v and the times of the direct exposure t_1 are shown on the left-hand side of each image pair, while the times of the delayed exposure t_2 can be calculated as $t_2 = t_1 + \Delta t$.

By using the shortest delay, i.e., $\Delta t = 300$ ps, the temporal origin of the plasma can be determined, as is shown in Fig. 2(a). In this case, the image illuminated by the direct pulse is empty, while the image exposed with the delayed pulse 300 ps later shows the plasma at the very beginning of the breakdown. It is clear that the

breakdown starts within this 300 ps time interval. With this technique, we are able to determine at which time during the excitation-laser pulse the average breakdown initiation occurs. The time zero in our experimental results corresponds to the average breakdown initiation. Since the breakdown is a statistical process, an individual breakdown can occur before or after our zero time.

The velocity measurements of the laser-induced plasma and the shock wave are shown on a log-log plot in Fig. 3. Here we measured the instantaneous axial velocities, v , of the plasma and the shock-wave evolution toward the excitation-laser radiation as a function of the time t after the breakdown initiation. The coordinate of an individual point (v, t) is calculated as

$$(v, t) = \left(\frac{d_2 - d_1}{\Delta t} \kappa, \frac{t_1 + t_2}{2} \right), \quad (1)$$

where d_1 and d_2 are the top positions (in pixels) of the observed phenomena on the direct and delayed images, separately, and $\kappa = 0.7 \mu\text{m}$ per pixel corresponds to the spatial resolution of the optical system. Since the measured axial velocities of the plasma development vary from 100 to 600 km/s in the first nanosecond after the breakdown initiation, we used the shortest delay, i.e., $\Delta t = 300$ ps, for this case [see also Figs. 2(b) and 2(c)]. Here, a significant measurement noise arises from the

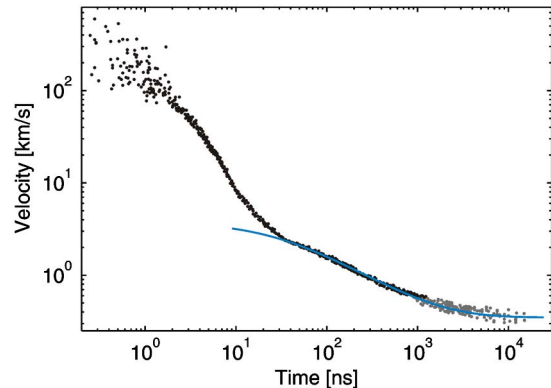


Fig. 3. (Color online) Axial velocity of the plasma and shock-wave evolution toward the excitation-laser radiation as a function of time t after the breakdown initiation. The solid curve shows the fit of the theoretical model for the spherical blast wave.

different mechanisms of plasma expansion [1,21]. The higher axial velocities (e.g., 300 km/s in Fig. 2(b)) correspond to the events recorded during the fast ionization, while the lower axial velocities are related to the events captured during the detonation wave (e.g., see Fig. 2(c) with $v = 120$ km/s).

When the fast ionization ends ($t \sim 2$ ns), the measurement noise in Fig. 3 is significantly reduced. Since the velocities of the plasma-driven shock wave are much lower than the velocities of the plasma development, the delay Δt should be appropriately prolonged. During our measurements, we were adapting the time delay Δt so that the difference $d_2 - d_1$ was in the range between 75 and 150 pixels. A typical image of the shock wave driven by the expansion of the high-pressure plasma is shown in Fig. 2(d). Here, the shock wave already has the ellipsoidal shape, and the measured axial velocity is 31 km/s. In our experiment, the excitation-laser radiation ends around 5 ns after the breakdown initiation.

Approximately 30 ns after the breakdown initiation, the plasma-driven shock wave is converted into a nearly spherical shock wave, as is clear from Fig. 2(e), captured at $t_1 = 55$ ns. The solid curve in Fig. 3 represents the theoretical velocity obtained by fitting the model for the spherical blast wave [20] to the data measured more than 30 ns after the breakdown initiation. Here, we used the standard conditions ($p = 10^5$ Pa, $T = 25^\circ\text{C}$) for air.

At times longer than $3\ \mu\text{s}$ the shock wave starts to convert into an acoustic wave and its velocity approaches the speed of sound, i.e., about 350 m/s. In this area, the measurement noise increases again due to a short delay line. Based on the assumption that the uncertainty in the image processing is five pixels, at least 25 pixels of difference between the top positions on both images are necessary for an error of less than 20%. Therefore, our experimental setup with the longest delay of $\Delta t = 30$ ns enables accurate measurements of velocities greater than 580 m/s. The measurements with lower velocities are marked with the gray dots in Fig. 3. In order to improve these measurements, a longer delay line should be used, which can be most appropriately realized with optical fibers.

If a longer time delay, e.g., $\Delta t = 5.5$ ns, is used at the very beginning of the breakdown, it is possible to observe how the plasma develops the shock wave. On the left-hand side of Fig. 2(f), the structure of the plasma at $t_1 = 400$ ps indicates that the breakdown occurs at different points within the excitation-beam volume. At later times, the blast waves propagating from local centers combine into a single shock wave, as can be seen from the image captured 5.5 ns later. However, an inappropriately long time delay Δt between both images gives an average velocity that does not conform to the instantaneous velocity, e.g., the axial (average) velocity v determined from Fig. 2(f) is 78 km/s, while the axial (instantaneous) velocity v for the corresponding time ($t = 3$ ns) is ~ 55 km/s (see Fig. 3).

In conclusion, we demonstrated that the developed method enables the 2D observation of a single, fast, laser-induced phenomenon in two time instances. Since

it uses two CCD cameras and a variable time delay between 30 ps-illuminations, it gives an insight into the plasma and shock-wave development within the nanosecond excitation-laser pulse as well as at later times. We point out that the time delay between successive images should be shorter than 1 ns to obtain the correct instantaneous velocities of the laser-induced-plasma development in air. Compared to the existing ultrahigh-speed 2D shadowgraphy, the presented method enables much shorter time delays, down to 300 ps, which can be further reduced by employing shorter illumination pulses. Therefore, it can be used for a detailed analysis of laser-induced breakdown, such as an analysis of the breakdown occurrence and the plasma evolution. Moreover, due to its simplicity, the developed method presents an easily accessible solution for many industrial and medical research-environments, where temporally and spatially resolved observation of different kinds of laser-induced phenomena in transparent media is required.

References

1. J. P. Singh and S. N. Thakur, *Laser-Induced Breakdown Spectroscopy* (Elsevier, 2007).
2. X. Zeng, X. Mao, S. S. Mao, S.-B. Wen, R. Greif, and R. E. Russo, *Appl. Phys. Lett.* **88**, 061502 (2006).
3. A. Vogel, *Phys. Med. Biol.* **42**, 895 (1997).
4. S. R. Aglyamov, A. B. Karpiouk, F. Bourgeois, A. Ben-Yakar, and S. Y. Emelianov, *Opt. Lett.* **33**, 1357 (2008).
5. M. Lackner, S. Charareh, F. Winter, K. F. Iskra, D. Rüdiger, T. Neger, H. Kopecek, and E. Wintner, *Opt. Express* **12**, 4546 (2004).
6. D. Kim, B. Oh, D. Jang, J.-W. Lee, and J.-M. Lee, *Appl. Surf. Sci.* **253**, 8322 (2007).
7. M. Kandula and R. Freeman, *Shock Waves* **18**, 21 (2008).
8. A. Vogel, I. Apitz, S. Freidank, and R. Dijkink, *Opt. Lett.* **31**, 1812 (2006).
9. A. Vogel, S. Busch, and U. Parlitz, *J. Acoust. Soc. Am.* **100**, 148 (1996).
10. J. Noack and A. Vogel, *Appl. Opt.* **37**, 4092 (1998).
11. S. Chaurasia, P. Leshma, S. Tripathi, C. G. Murali, D. S. Munda, S. M. Sharma, and S. Kailas, *BARC Newsletter* **317**, 13 (2010).
12. Z. Liu, G. J. Steckman, and D. Psaltis, *Appl. Phys. Lett.* **80**, 731 (2002).
13. P. Gregorčič, R. Petkovšek, and J. Možina, *J. Appl. Phys.* **102**, 094904 (2007).
14. H. Sobral, M. Villagrán-Muniz, R. Navarro-González, and A. C. Raga, *Appl. Phys. Lett.* **77**, 3158 (2000).
15. R. Gaudiuso, M. Dell'Aglio, O. De Pascale, G. S. Senesi, and A. De Giacomo, *Sensors* **10**, 7434 (2010).
16. Y. Liu, J. S. Penczak, and R. J. Gordon, *Opt. Lett.* **35**, 112 (2010).
17. T. Perhavec and J. Diaci, *Strojniški Vestnik—J. Mech. Eng.* **56**, 477 (2010).
18. E. A. Brujan, T. Ikeda, K. Yoshinaka, and Y. Matsumoto, *Ultrason. Sonochem.* **18**, 59 (2011).
19. G. E. Busch and G. Charatis, *Proc. SPIE* **348**, 650 (1982).
20. D. L. Jones, *Phys. Fluids* **11**, 1664 (1968).
21. A. A. Ilyin, I. G. Nagorny, and O. A. Bukin, *Appl. Phys. Lett.* **96**, 171501 (2010).
22. Y. B. S. R. Prasad, S. Barnwal, P. A. Naik, J. A. Chakera, R. A. Khan, and P. D. Gupta, *Appl. Phys. Lett.* **96**, 221503 (2010).